Front. Earth Sci. 2022, 16(4): 846–864
https://doi.org/10.1007/s11707-021-0950-5

RESEARCH ARTICLE

Warming hiatus of extreme temperature across China's cold regions during 1998–2018

Luo MA[1,2], Ruijie LU (✉)[1,2], Dongxue CHEN[1,2]

1 Engineering Center of Desertification and Blown-Sand Control (Ministry of Education), Faculty of Geographical Science, Beijing Normal University, Beijing 100875, China
2 Key Laboratory of Environmental Change and Natural Disaster (Ministry of Education), Faculty of Geographical Science, Beijing Normal University, Beijing 100875, China

Abstract The recent hiatus in global warming has attracted significant attention, yet whether it is a widespread global and/or regional phenomenon remains controversial. Here, we investigate the response of extreme temperature changes since 1961 across China's cold regions (CCR): Tibetan determine the spatiotemporal characteristics of extreme temperature changes across these cold regions using Mann-Kendall and wavelet transform coherence (WTC) analyses of data from 196 meteorological stations from 1961 to 2018. We further investigate the teleconnection between extreme temperatures and large-scale ocean-atmosphere circulation to determine the potential synoptic scale causes of the observed changes. The results revealed a significant warming slowdown in all extreme temperature indices across CCR from 1998 to 2018. In addition, extreme temperature indices in northwest cold region (NWC) and north cold region (NC) reveal a clear winter warming slowdown and even a significant cooling trend, yet only the cold index in Tibetan Platean cold region (TPC) shows a warming hiatus. We conclude that the warming hiatus observed across these regions is primarily driven by extreme temperature index changes in winter. We also find that phase variations in the Atlantic Multi-decadal Oscillation (AMO) and Arctic Oscillation (AO) critically impact on the observed warming hiatus, but the specific atmospheric mechanisms are elusive and warrant further analysis and investigation.

Keywords China's cold regions, warming hiatus, wavelet transform coherence, ocean-atmosphere circulations

1 Introduction

The Fifth Assessment Report of the Intergovernmental Panel on Climate Change (IPCC AR5) indicates that the global mean surface air temperature increased by 0.85°C (0.65°C–1.06°C) from 1901 to 2012, with a more significant warming trend since the 1950s (IPCC, 2014). Numerous studies link global warming with increases in extreme weather events, such as floods (Donat et al., 2016; Bubeck et al., 2019), droughts (Diffenbaugh et al., 2017; Wang et al., 2019) and extreme heat waves (Fenner et al., 2019), that will have important socio-economic impacts as well as driving profound ecological changes (Curtis et al., 2017; Li et al., 2019).

However, some studies have indicated that global-mean surface air temperatures (GMSTs) have not increased continuously since 1998 (Medhaug et al., 2017). IPCC AR5 has suggested that the GMSTs increased at a rate of 0.05°C per decade during 1998–2012 and 0.12°C per decade from 1951 to 2012. This slowing down in the warming trend of GMSTs after the late-1990s has been termed a "warming slowdown", "hiatus" or "pause" (Fyfe et al., 2013 and 2016; Slingo, 2013; Medhaug et al., 2017). Numerous studies have confirmed this warming hiatus over both global (Johnson et al., 2018; Winslow et al., 2018) and regional scales (Garfinkel et al., 2017; Shen et al., 2018) based on model simulations and observational data records (Easterling and Wehner, 2009; Kerr, 2009; IPCC, 2014; England et al., 2014). Yet, some studies have argued that there has been no global warming hiatus since 1998 (Karl et al., 2015; Rajaratnam et al., 2015; Huang et al., 2017a). The discrepancies between these studies may be due to different start dates and to their partitioning of temperature records (Karl et al., 2015; Rajaratnam et al., 2015). In addition, significant differences between climate model predictions and observations remain a source of debate with respect to a global warming slowdown (Trenberth, 2015; Zhang, 2016; Huang et al., 2017b). Although the GMSTs warming hiatus is uncertain, the hiatus is consistent with most observations (Easterling and Wehner, 2009; Fyfe et al.,

Received April 14, 2021; accepted September 1, 2021

E-mail: ruijielu@bnu.edu.cn

2013; Medhaug et al., 2017).

China cold regions (CCR) is located at high latitudes or high altitude, and includes Tibetan Plateau cold region (TPC), northwest cold region (NWC) and north cold region (NC) (Yang et al., 2000; Chen et al., 2006). These cold regions are characterized by high levels of stored precipitation in the form of ice or snow, and provide important water resources for arid and semi-arid regions (Shen et al., 2020; Shen et al., 2021; Wang et al., 2021). Furthermore, these cold regions are also important areas of animal husbandry in China, and NC is a commercially important grain-growing center (Ding et al., 2019a, 2019b; Zhou et al., 2020). Cold, highland regions can be extremely sensitive to climate change, due to their complex natural environment and fragile ecosystems (Li and Cheng, 1999). Some studies indicate that the frequency of extreme temperature events across high latitude/altitude regions such as Tibetan Plateau and northwest China in the context of global warming, is significantly higher when compared to other parts of China (Guo et al., 2018; Zhu et al., 2018). In addition, the accelerated warming of cold regions has caused a series of ecological and environmental problems, such as rapid melting and retreat of glaciers, glacial lake outburst floods, and natural disasters such as landslides, mudslides, and floods. Hence, in terms of defining current and future risk to natural hazards, it is important to understand temperature changes – particularly the extremes – across cold regions (Qin et al., 2018; Ding et al., 2019a).

Previous studies have mainly focused on the analysis of spatiotemporal variations in climatic factors (Chen and Sun, 2015; Wen et al., 2017) and few studies have concentrated on extreme temperature changes in cold regions since the late 1990s. In addition, the influence of atmospheric circulation patterns has important significance for any regional warming hiatus (Swain et al., 2016; Diffenbaugh et al., 2017), and has provided a basis for projecting future regional extreme climate changes. However, in these previous studies, there is little discussion of the relationship between regional extreme temperature and large-scale ocean-atmosphere circulation patterns, while it remains controversial as to whether or not a warming hiatus has been observed, particularly across CCR and most notably TPC (An et al., 2016; Cai et al., 2017).

Compared with the annual mean temperature, the extreme temperature index can better reflect the overall state of the climate system, especially the variability of extreme temperature events (Alexander et al., 2006; Li and Zha, 2018). Therefore, studying variations in the extreme temperature index since 1998 not only reveals whether the climate system has undergone a warming hiatus during this period, but also reflects the differences in the internal changes of the climate system in different regions from various aspects (Ding et al., 2020).

In this study, we analyze meteorological data from 1961 to 2018 across the three cold regions to: (i) compare the temporal variation and spatial distribution of temperature index between 1961 and 1997 and 1998–2018; (ii) discuss correlations between latitude, longitude, altitude and extreme temperature index using Pearson correlation analysis; and (iii) explore the relationship between the observed trends and synoptic scale ocean-atmosphere circulation patterns.

2 Material and methods

2.1 Study area

The three cold regions studied here (TPC, NWC and NC) have a total area of 4.17×10^6 km^2, and account for 43.5% of China's total land area (Fig. 1). The regions are characterized by high altitude and latitude, with the lowest monthly mean temperature of less than −3°C and annual mean temperature less than 5°C. Fewer than 5 months have a mean temperature greater than 10°C (Yang et al., 2000; Chen et al., 2006). The Tibetan Plateau, known colloquially as the "roof of the world" and "Chinese water tower", is the highest upland cold region in the world, with a total area of 2.62×10^6 km^2. It has an important impact on regional and global atmospheric circulation and is a hotspot of global climate change (Wang et al., 2013). NWC lies mainly in the Altay Mountains and Tienshan Mountains, and has an area of 2.1×10^6 km^2. NWC, located deep in the hinterland of Eurasia, is characterized by a fragile ecology and complex natural environment and is one of the most sensitive areas to global climate change (Chen et al., 2014; Ding et al., 2019a). NC is composed of the Northeast Plain and Daxinganling Mountains, has the highest mean latitude and the lowest mean temperature in China, and covers a total area of 1.34×10^6 km^2. NC spans both monsoon and non-monsoon climatic regions and is an important production base for agriculture and animal husbandry in

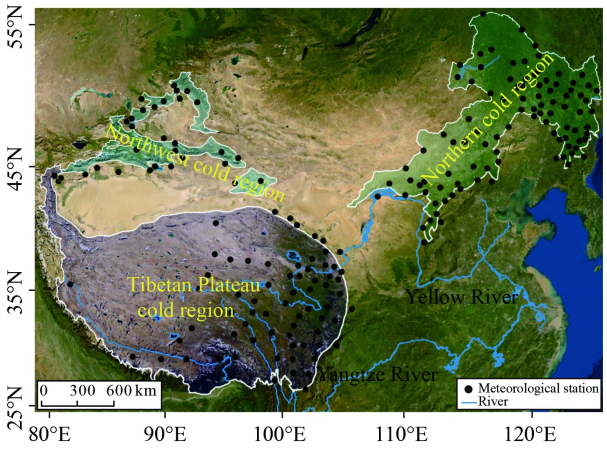

Fig. 1 The three main cold regions analyzed in this study, and location of the 196 meteorological stations used in this study.

China. Extreme temperatures have a major impact on regional agricultural production (Fu et al., 2018; Tong et al., 2019) and in the past 50 years, this region has been one of the fastest warming regions in China and East Asia (Ren et al., 2012).

2.2 Data sources and quality control

We used meteorological data from 206 weather stations obtained from the China Meteorological Administration (available at China Meteorological Administration website). Data included daily mean, minimum and maximum temperatures over the period of 1961–2018. To ensure the reliability of the data record, we eliminated 10 weather stations that had missing data over a year or more. For the remaining stations, data gaps (< one year) were interpolated based on data from the nearest station. In total, 196 weather stations with complete data records were used in the study.

The Atlantic Multi-decadal Oscillation (AMO) (available at National Oceanic and Atmospheric Administration website) is considered as an important large-scale indicator of climate change in the Northern Hemisphere (Chen and Tung, 2014). In addition, the Arctic Oscillation (AO) (available at National Oceanic and Atmospheric Administration website) shows seesaw behavior in the Northern Hemisphere, that is, when the AO is in its negative phase, strong northerly wind anomalies are observed in the lower troposphere. These transport cold air from high latitudes to low latitudes, resulting in lower temperature in the middle latitudes (Song and Wu, 2019). Therefore, we choose the AMO and AO in this study to more fully understand the mechanisms driving climate changes (You et al., 2013; Deng et al., 2014; Huang et al., 2016).

2.3 Methodology

2.3.1 Definition of extreme index

To compare temperature changes over the study period 1961–2018 across the three regions, maximum and minimum temperatures and a further four extreme temperature indices were calculated using the RClimDex 1.9 software package (Zhang et al., 2011; Supari et al., 2017; Ding et al., 2020; Niu et al., 2020). Since other studies have focused more on TXm, TNm, TX90p, TNx, TN10p and TNn, the six total temperature indices (Table 1) were selected from the core index recommended by the CCI/CLIVAR/JCOMM Expert Team on Climate Change Detection to include (i) annual temperature index: the annual mean maximum and minimum temperature (TXm and TNm); (ii) warm extreme daily temperature index: the percentage of days when TX is greater than the 90th percentile of warmest days, and monthly maximum value of daily minimum temperature (TX90p and TNx); (iii) cold extreme temperature index: the percentage of days when TN is lower than the 10th percentile of coolest daily temperature, and monthly minimum value of daily minimum temperature (TN10p and TNn) (Li et al., 2015; Shen et al., 2018).

2.3.2 Mann-Kendall trend analysis

A nonparametric Mann-Kendall (M-K) test is recommended to detect monotonic trends in hydrometeorological time-series across different regions of the world (Huang et al., 2017b; Ding et al., 2018; Pakalidou and Karacosta, 2018; Ding et al., 2019b). The magnitude of test statistic Z represents the significance level, $Z > 0$ indicates an increase, and $Z < 0$ indicates a decrease. When $|Z| > 1.96$ and $|Z| > 2.58$, the trends are significant at the 95% and 99% confidence level, respectively (Ding et al., 2018; Niu et al., 2020). In addition, the nonparametric Sen's slope method can complement the M-K trend analysis by quantifying the magnitudes of trends of extreme temperature index (Sen, 1968; Guo et al., 2018). Finally, we define our meteorological seasons as spring (March to May, MAM), summer (June to August, JJA), autumn (September to November, SON), and winter (December to February, DJF).

Table 1 The six temperature indices used in this study

Index	Indicator name	Definitions	Units
Annual mean temperature			
TXm	Mean TX	Mean daily maximum temperature	°C
TNm	Mean TN	Mean daily minimum temperature	°C
Warm temperature extremes			
TX90p	Warm days	Percentage of days when TX > 90th percentile	d
TNx	Max TN	Monthly maximum value of daily minimum temperature	°C
Cold temperature extremes			
TN10p	Cool nights	Percentage of days when TN < 10th percentile	d
TNn	Min TN	Monthly minimum value of daily minimum temperature	°C

Notes: TX is daily maximum temperature; TN is daily minimum temperature.

2.3.3 Wavelet transform coherence (WTC)

WTC has been previously used to detect the interactions and feedback characteristics of extreme temperature variations and large-scale ocean-atmosphere circulation patterns (Ding et al., 2020). WTC is an effective method to measure the correlation between two independent signals in the local time and frequency domains (Torrence and Compo, 1998; Jevrejeva et al., 2003; Grinsted et al., 2004). Following Torrence and Compo (1998), the WTC is defined as

$$R_n^2(s) = \frac{\left|S\left(s^{-1}W_n^{XY}(s)\right)\right|^2}{S\left(s^{-1}\left|W_n^X(s)\right|^2\right)\times S\left(s^{-1}\left|W_n^Y(s)\right|^2\right)}, \quad (1)$$

where W_n^X and W_n^Y are transformed from the time series by X and Y, and S is a smoothing function. The scales in time and frequency over which S is filtered, define the scales over which coherence is a measure of the covariance similar to a traditional correlation coefficient (Jevrejeva et al., 2003). WTC defines the ratio of the cross product of the amplitudes of two time-series at a given frequency to the amplitude product of each wave. The smoothing operator S is defined as

$$W_n^{XY}(s) = W_n^X(s)\times W_n^{Y*}(s), \quad (2)$$

where * denotes the complex conjugate. R_n^2 returns a value between zero and unity, where 0 indicates no correlation, and 1 indicates a perfect correlation. The relevant code and the calculation procedure can be found at National Oceanography Centre website.

3 Results

3.1 Temporal variations in annual mean temperature (TXm and TNm)

From 1961 to 2018, the annual mean maximum (TXm) and minimum (TNm) temperature increased significantly ($P < 0.01$) across CCR, by 0.23°C and 0.43°C per decade, respectively (Figs. 2(a) and 2(b)). For each of the cold regions, TXm and TNm also showed clear increasing trends: 0.30°C and 0.40°C per decade for TPC, 0.21°C and 0.47°C per decade for NWC, and 0.22°C and 0.44°C per decade for NC (Figs. 3(a)–3(f)).

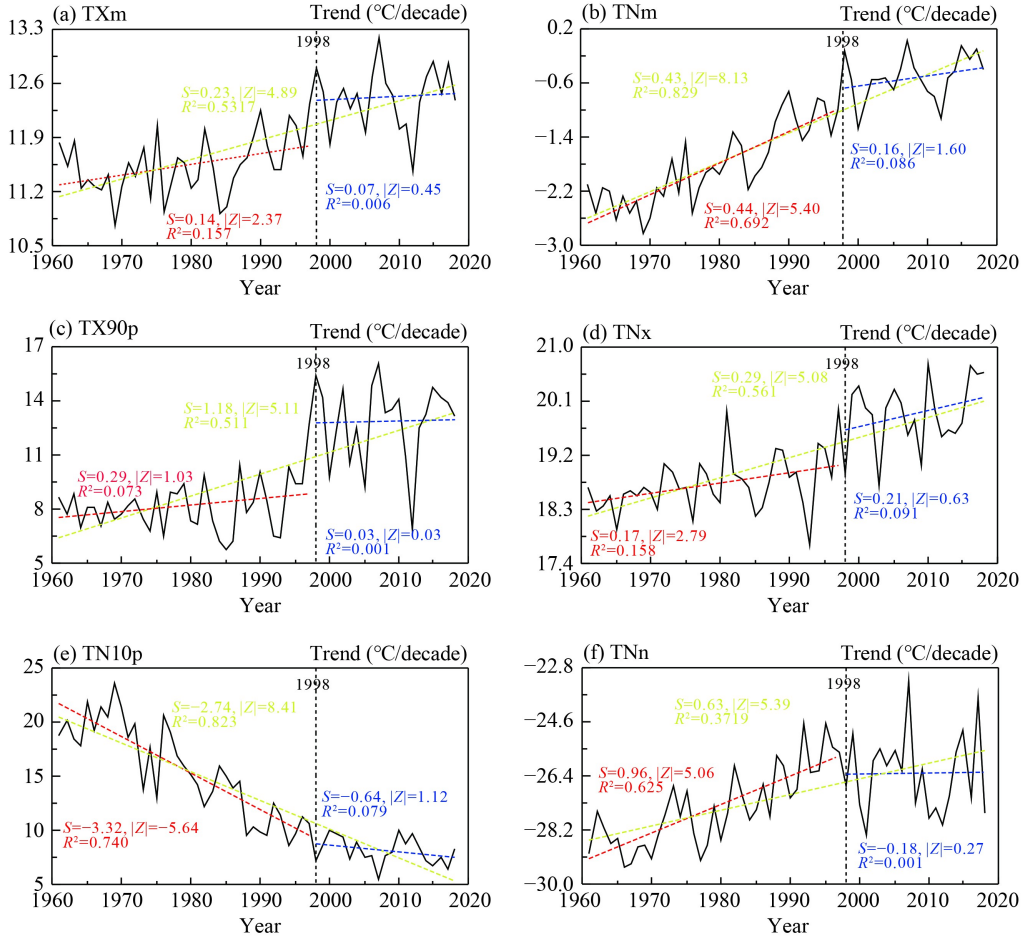

Fig. 2 Annual mean time series of six temperature indices in CCR.

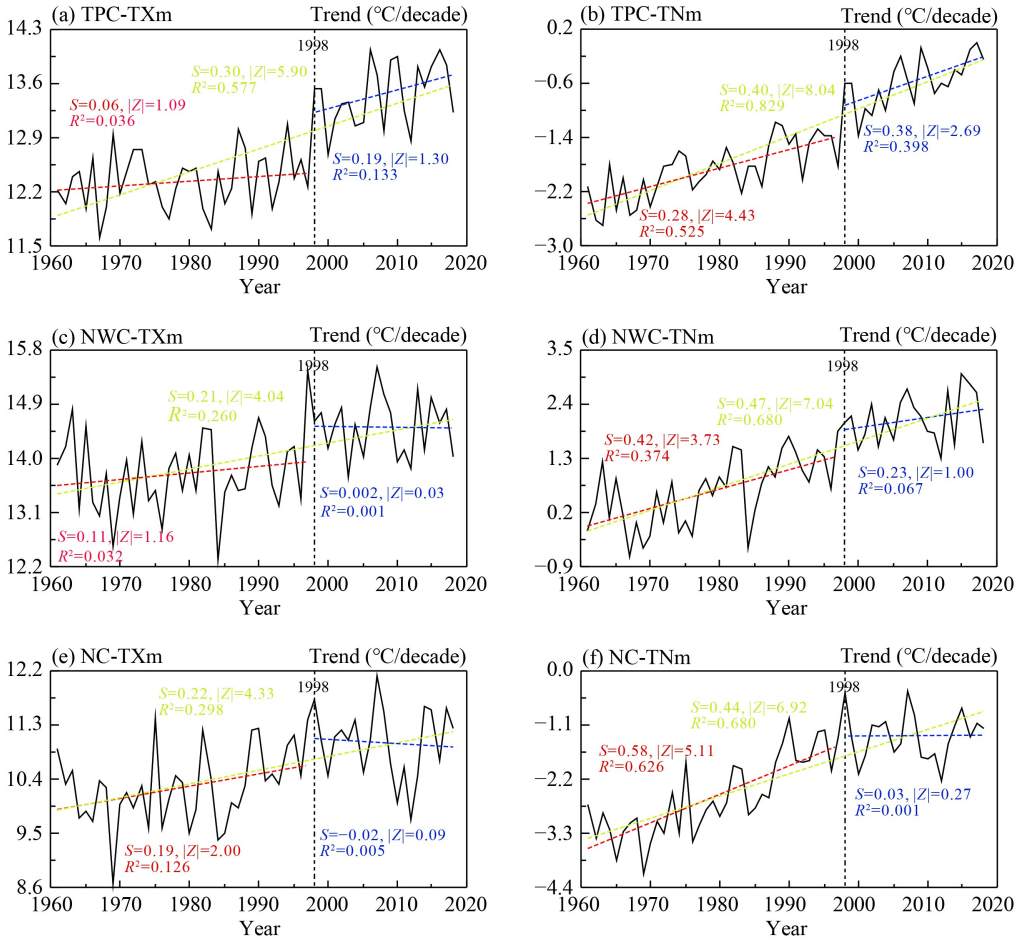

Fig. 3 Annual mean TXm and TNm time series in three cold regions.

During the period 1961–1997, TXm and TNm across all cold regions increased by 0.14°C and 0.44°C per decade, respectively (Figs. 2(a) and 2(b)). Regionally, TXm across TPC and NWC increased slightly at 0.06°C and 0.11°C per decade, but TNm increased significantly at 0.28 and 0.42°C per decade, respectively (Figs. 3(a)–3(d)). In contrast, across NC, TXm and TNm increased significantly at rates of 0.19 and 0.58°C per decade (Figs. 3(e) and 3(f)).

Compared with 1961–1997, the more recent extreme temperature trends from 1998 to 2018 are substantially different. TXm and TNm increased at slower rates of 0.07 and 0.16°C per decade in CCR (Figs. 2(a) and 2(b)), and for the NWC and NC regions, TXm and TNm actually showed a slowdown in warming (Figs. 3(c)–3(f)). However, the two indices showed significant accelerating warming trends across TPC (Figs. 3(a)–3(b)). Based on this analysis, with the exception of TPC we found that the warming trend in annual mean temperature across CCR over the past 21 years slowed down, or even reversed, compared with 1961–1997. This trend is consistent with the global warming hiatus (Slingo, 2013). By comparing the different trends in TXm and TNm across the three cold regions, it can be inferred that the mean temperature increase was predominantly affected by NWC and NC. These results are similar to those of Duan and Xiao (2015), who revealed that the annual mean temperature continued to rise across Tibetan Plateau despite the global warming hiatus.

3.2 Annual mean trend variability of warm extremes (TX90p and TNx)

Over the past 58 years, the warm index has followed an obvious increasing trend across CCR (Figs. 2(c) and 2(d)). Among the temperature indices, two stand out (TX90p for TPC and TNx for NC) as the fastest rising, at 1.54 days per decade and 0.34°C per decade, respectively (Figs. 4(a)–4(f)). In contrast, TNx for TPC and TX90p for NC had the slowest warming rate among the three cold regions, at 0.32°C per decade and 0.89 days per decade (Figs. 4(b)–4(e)).

From 1961 to 1997, almost all the warm extreme indices across the three cold regions demonstrate low, insignificant ($P > 0.05$) increases, with only TNx in NWC showing a significant ($P < 0.01$) temperature increase at 0.23°C per decade (Figs. 4(a)–4(d)). It is noteworthy that in this latter period, the warm extremes across all three

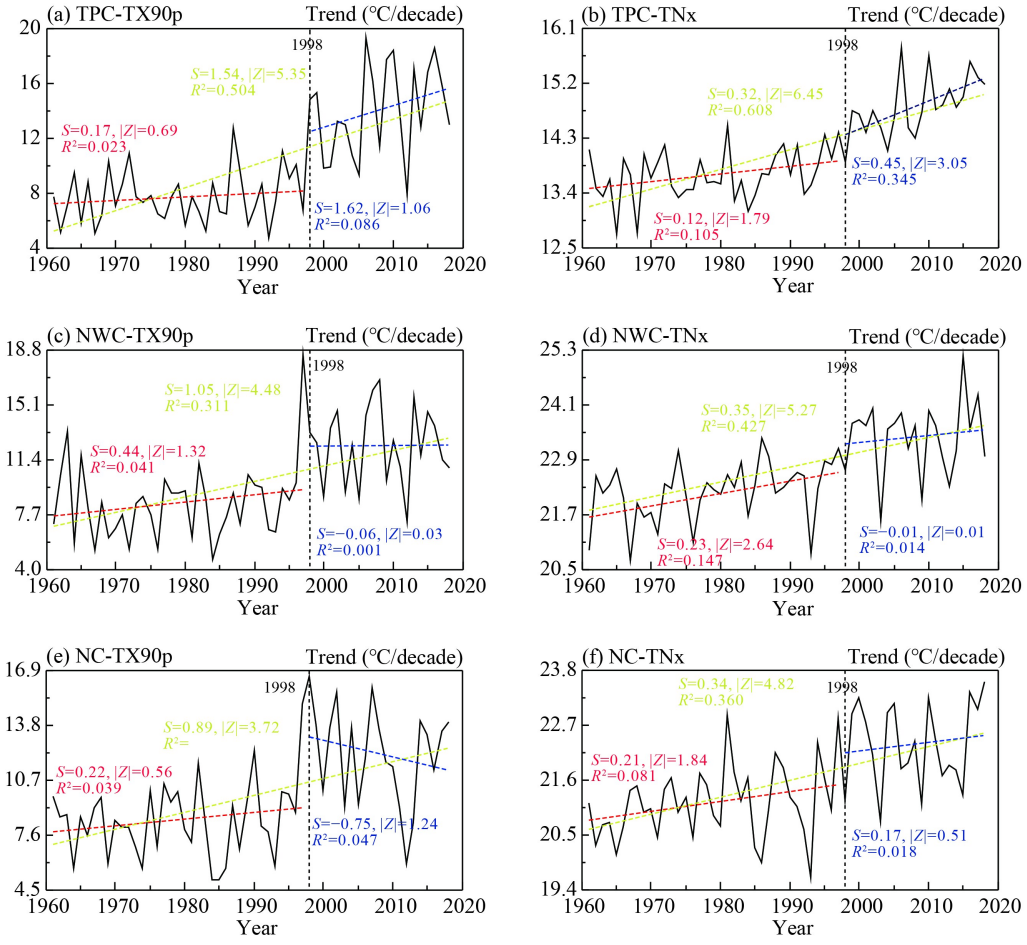

Fig. 4 Annual mean trends of warm extremes across the three cold regions.

cold regions showed markedly different trends from the previous period (1961–1997). TX90p and TNx across the TPC increased rapidly, at rates of 1.63 days per decade and 0.45°C per decade, respectively. Compared with the previous period, the overall magnitude of the warming strengthened significantly (Figs. 4(a) and 4(b)). TX90p and TNx across NWC and NC showed an insignificant cooling trend with the exception of TNx across NC, which increased at a rate of 0.17°C per decade (Figs. 4(c)–4(f)). Furthermore, TX90p across CCR showed a warming slowdown of 0.03 days per decade, while TNx indicates strengthened warming of 0.21°C per decade (Figs. 4(c) and 4(d)).

In general, during the warming slowdown period from 1998 to 2018, the warm extremes in NWC and NC showed a decreasing rate of warming, while TPC showed an accelerating warming trend.

3.3 Annual mean trend variability of cold extremes (TN10p and TNn)

From 1961 to 2018, the cold extremes across all three cold regions demonstrate significant ($P < 0.01$) warming trends. Among them, TN10p showed the most obvious warming trend of 2.83 days per decade across TPC, followed by 2.50 days per decade across NC and 2.48 days per decade across NWC (Figs. 5(a), 5(c), and 5(e)). For TNn, the most rapid increase was 0.57°C per decade across NWC, followed by 0.52°C per decade for the TPC and 0.51°C per decade across NC (Figs. 5(b), 5(d), and 5(f)). Across the entire cold regions, TN10p and TNn increased significantly at 2.74 days per decade and 0.63°C per decade, respectively (Figs. 2(e) and 2(f)).

From 1961 to 1997, TN10p and TNn in all three cold regions showed significant warming trends ($P < 0.01$). Specifically, the variation in magnitude of TN10p from the highest to the lowest was across NC at 4.01 days per decade, TPC at 2.91 days per decade and NWC at 2.76 days per decade (Figs. 5(a), 5(c), and 5(e)). For TNn, the fastest warming was in NWC at 1.31°C per decade, followed by NC at 1.15°C per decade and TPC at 0.58°C per decade (Figs. 5(b), 5(d), and 5(f)). By contrast, during the period after 1998 coeval with warming slowdown, the variations of the cold extremes across all regions were significantly lower than those in the previous period. In particular, TN10p across NWC decreased by just 0.33 days per decade, significantly lower than the 2.76 days per decade during the previous period (Fig. 5(c)). TN10p

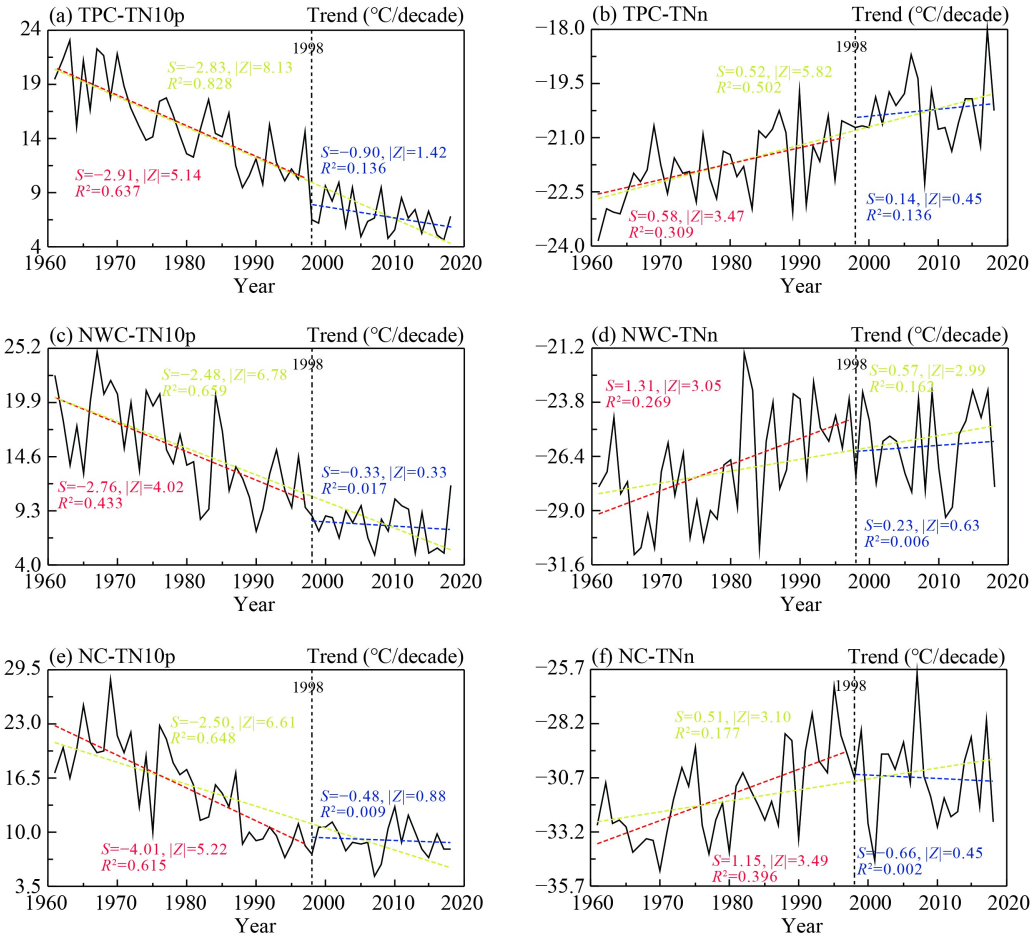

Fig. 5 Annual mean trends of cold extremes across the three cold regions.

and TNn across all regions also displayed strong cooling trends from 1998 to 2018, at 0.64 days per decade in TN10p and 0.18°C per decade in TNn, respectively, far lower than the previous period at 3.32 days per decade and 0.96°C per decade, respectively. The trends in our data indicate that the cold extremes across all three cold regions have shown a distinct warming slowdown trend in the past 20 years.

3.4 Seasonal trend variability of temperature extremes

Our previous analysis demonstrates that, on the annual time-scale, the cold indices and warm indices all exhibited clear regional differences during the period of the warming slowdown (1998–2018). On this basis, we further analyze the trends in extreme temperature indices on a seasonal time-scale. From 1961 to 1997, TX90p across all three cold regions revealed a significant warming trend both in summer and winter, except for NC which had an insignificant cooling trend in summer (Fig. 6). The largest warming (TX90p = 1.35 days per decade) occurred across NWC in winter (Fig. 6(f)). The lowest warming trend for TX90p occurred across NWC at 0.25 days per decade in summer (Fig. 6(e)). TNx reveals warming trends in winter and summer across all three cold regions. It is noteworthy that the warming magnitude of TNx in winter across the three cold regions (0.47°C per decade for TPC, 0.50°C per decade for NWC and 0.76°C per decade for NC) (Figs. 6(d), 6(h), and 6(l)) were higher than those in summer (0.19°C per decade for TPC, 0.15°C per decade for NWC and 0.16°C per decade for NC) (Figs. 6(c), 6(g), and 6(k)).

In contrast, the warm seasonal extremes from 1998 to 2018 had markedly different responses. Among them, TX90p and TNx showed warming trends in summer of 3.12 days and 0.49°C per decade for TPC, 0.69 days and 0.18°C per decade for NWC and 0.09°C per decade for NC (Fig. 6). In winter, except for warming trends in TPC at 0.74 days per decade and 0.45°C per decade (Figs. 6(b) and 6(d)), TX90p and TNx showed cooling trends across the two other cold regions at 2.49 days per 0.38°C per decade, and 0.17 days per decade (Figs. 6(f), 6(h), and 6(j)). In general, for CCR during the period 1998–2018, the warm extremes showed significant warming slowdown and even significant cooling in winter. However, in summer, the warm extremes across the three cold regions showed an increasing warming trend except across NC.

We note that cold extremes across the three regions

showed an obvious warming slowdown and cooling trend in winter and summer from 1998 to 2018, with the exception of the TN10p and TNn indices across the TPC, which continued to warm at rates of 1.81 days per decade and 0.40°C per decade during summer (Figs. 6(a) and 6(c)). From 1961 to 1997, TN10p in NWC reveals a warming trend of 2.77 days per decade and 3.71 days per decade for the summer and winter seasons, respectively. However, the warming rates (TN10p) in NWC for the latter (1998–2018) period were just 1.08 days per decade and 2.02 days per decade, respectively (Figs. 6(e) and 6(f)). Likewise, for NC from 1961 to 1997, TNn showed warming of 0.55°C and 1.32°C per decade in summer and winter, respectively, while from 1998 to 2018, TNn revealed consistent winter and summer cooling rates of 0.07°C per decade (Figs. 6(k) and 6(l)).

3.5 Spatial distributions of temperature extreme trends

For each meteorological station, we determined whether each temperature index has a statistically significantly trend over the two periods, 1961–1997 and 1998–2018 (Tables 2 and 3). The annual mean TXm shows a warming trend across all three cold regions, in which a total of 164 stations demonstrated statistically significant warming trends. These were mostly in northeastern TPC, northern NWC, and NC from 1961 to 1997 (Table 2, Fig. 7(a)). Almost all of the stations across NC showed a positive warming trend, with 34 stations showing significant increases. Furthermore, we found 20 stations with a statistically weak cooling trend in southeastern TPC, just three of which were significant at the 5% level. However, from 1998 to 2018, we found continuously warming trends across TPC and eastern NWC at 73 stations, while cooling was observed at 77 stations across other regions, mainly located in southeastern and southwestern NC, and western NWC (Table 3, Fig. 7(b)).

In terms of TNm, 159 stations showed a significant increase with a warming rate that exceeded 0.5°C per decade in eastern TPC, northern NWC and eastern NC from 1961 to 1997 (Table 2, Fig. 7(c)). Furthermore, 12 stations showed a negative trend across all three cold regions, but most of these were insignificant at the 5% level. In contrast, during the latter period of warming slowdown, 138 stations with significantly continuous warming trends were predominantly located across the TPC and NC, while 58 stations indicating cooling were mainly distributed in southwestern NC (Table 3, Fig. 7(d)).

For our TX90p index, a total of 128 stations reveal a warming trend; these were predominantly located in

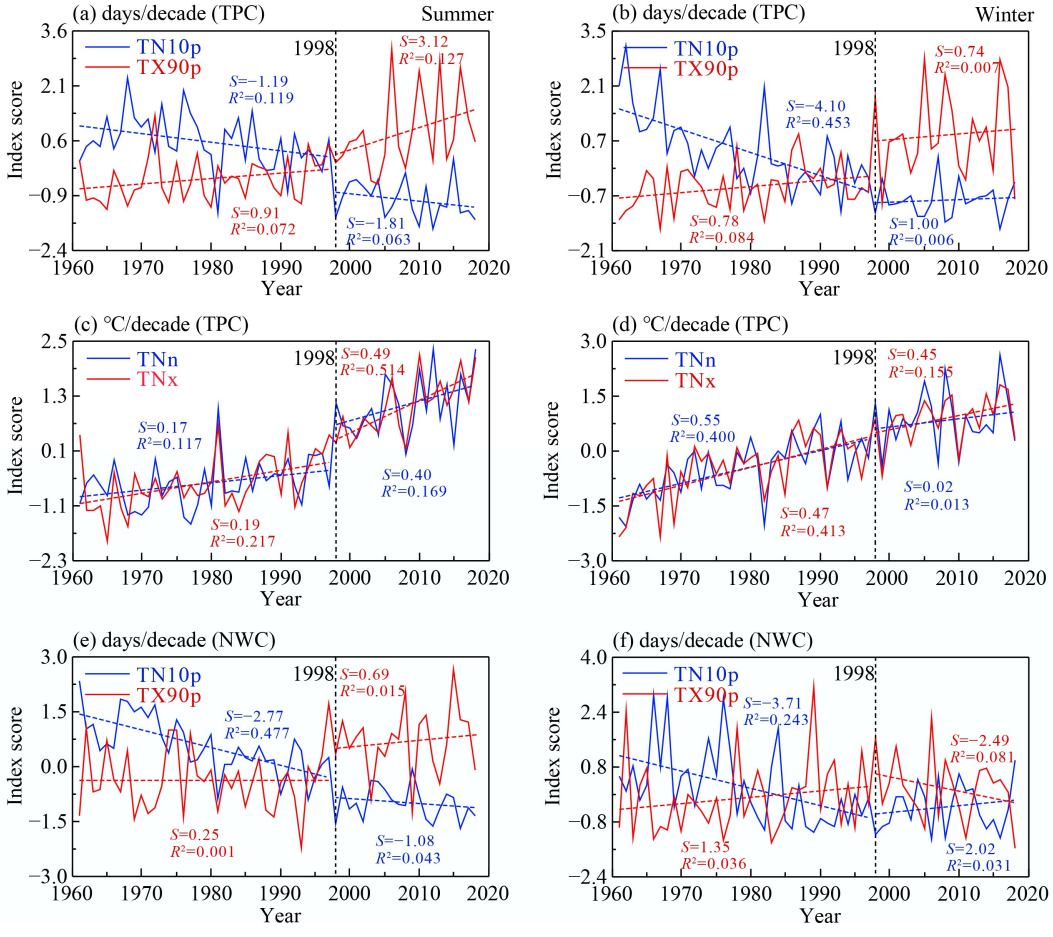

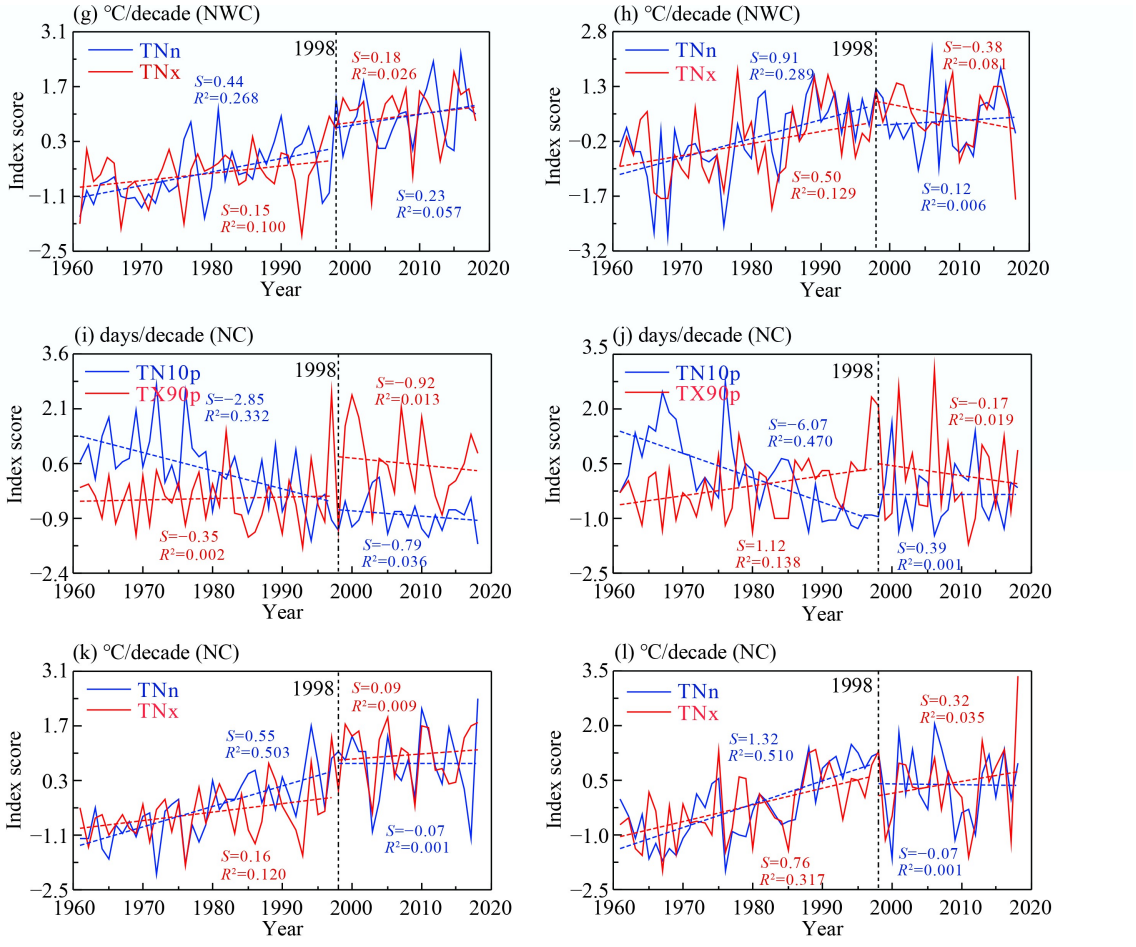

Fig. 6 Inter-comparison of warm and cold trends from 1961 to 2018 across each of the three cold regions.

northwestern TPC, western NWC and eastern NC (Table 2, Fig. 7(e)). However, 62 stations also indicate cooling, and these were mostly distributed in southeastern TPC and central and western NC. During the latter period (1998–2018), TX90p showed warming trends at 58 stations across TPC, but in contrast, 85 stations indicated cooling in western NWC and across most of NC (Table 3, Fig. 7(f)).

For TNx, except for TPC, the distribution of cooling and warming was entirely consistent with TX90p for the early (1961–1997) period. The majority (142) of stations with a warming trend were located in TPC, northern NWC and eastern NC (Table 2, Fig. 8(a)). A further 38 stations indicating cooling were distributed across northeastern TPC, central and southern NWC and central and southern NC. During the latter period (1998–2001), coinciding with the warming hiatus, TNx indicates cooling or insignificant warming trends across most of the cold regions, although TPC experienced continuous warming (Table 3, Fig. 8(b)).

Mean annual TN10p index yields a decrease across CCR from 1961 to 1997. A total of 186 stations with significant warming at the 5% level were located across TPC, NWC and NC (Table 2, Fig. 8(c)). However, just 141 stations showed similar warming from 1998 to 2018,

Table 2 Stations demonstrating a statistically significant temperature trends from 1961 to 1997 (S stands for significance at 0.05)

Index	TPC			NWC			NC			CCR		
	Decreasing trend (S)	Increasing trend (S)	No trend	Decreasing trend (S)	Increasing trend (S)	No trend	Decreasing trend (S)	Increasing trend (S)	No trend	Decreasing trend (S)	Increasing trend (S)	No trend
TXm	20(3)	46(11)	2	6(0)	22(2)	3	1(0)	96(34)	0	27(3)	164(47)	5
TNm	5(2)	63(47)	0	4(0)	27(23)	0	3(0)	94(89)	0	12(2)	184(159)	0
TX90p	26(2)	38(9)	4	5(0)	26(4)	0	31(0)	64(7)	2	62(2)	128(20)	6
TNx	15(2)	48(17)	5	9(1)	20(10)	2	14(0)	74(16)	9	38(3)	142(43)	16
TN10p	63(48)	5(2)	0	29(20)	2(0)	0	94(90)	3(0)	0	186(158)	10(2)	0
TNn	9(3)	57(32)	2	0(0)	31(22)	0	0(0)	97(70)	0	9(3)	185(124)	2

Table 3 Stations demonstrating statistically significant temperature trends from 1998 to 2018 (S stands for significance at 0.05)

Index	TPC			NWC			NC			CCR		
	Decreasing trend (S)	Increasing trend (S)	No trend	Decreasing trend (S)	Increasing trend (S)	No trend	Decreasing trend (S)	Increasing trend (S)	No trend	Decreasing trend (S)	Increasing trend (S)	No trend
TXm	11(1)	56(16)	1	14(1)	17(1)	0	52(1)	44(0)	1	77(3)	117(17)	2
TNm	9(2)	59(34)	0	10(0)	21(6)	0	39(14)	58(11)	0	58(16)	138(51)	0
TX90p	10(0)	58(6)	0	15(1)	16(1)	0	70(4)	27(0)	0	95(5)	101(7)	0
TNx	6(0)	57(26)	5	12(1)	17(3)	2	29(2)	60(3)	8	47(3)	134(32)	15
TN10p	50(28)	18(3)	0	23(4)	8(0)	0	68(16)	28(10)	1	141(48)	54(13)	1
TNn	24(4)	42(5)	2	14(0)	17(1)	0	62(9)	33(7)	2	100(13)	92(13)	4

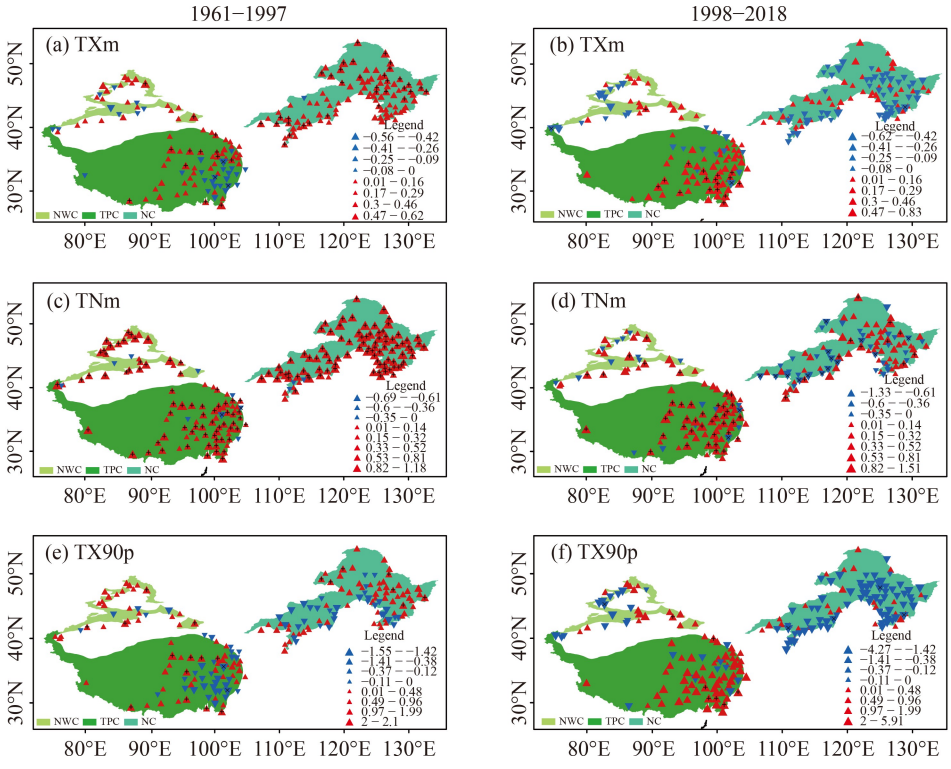

Fig. 7 The spatial distribution of annual warming temperature trends between 1961–1997 and 1998–2018 for (a) (b) TXm, (c) (d) TNm and (e) (f) TX90p.

showing that TN10p indicated a warming slowdown across northeastern TPC, southwestern NWC and NC (Table 3, Fig. 8(d)).

The warming trend revealed by TNn is also clear, with 185 stations showing a substantial increase, and many stations with a trend exceeding 0.92°C per decade in eastern TPC, northern NWC and all of NC from 1961 to 1997 (Table 2, Fig. 8(e)). Furthermore, there was slight cooling across western TPC, with 3 stations indicating a significant trend. From 1998 to 2018, TNn exhibited a stronger cooling trend across most of NC and parts of other cold regions. Compared with annual mean TNn from 1961 to 1997, there were fewer stations (92) showing a net increase across all three cold regions from 1998 to 2018 (Table 3, Fig. 8(f)).

Our observations of temperature index from 1961 to 2018 demonstrate that China's three cold regions experienced a warming hiatus during 1998–2018, with the notable exception of TPC, which continued to warm. Moreover, compared with the other regions, central and western NWC and NC reflected the strongest response to the hiatus, while southeastern TPC was most sensitive to observed climate change.

4 Discussion

We find that the overall warming trend from 1961 to 2018 reflected in our extreme temperature indices across the CCR was generally consistent with the net warming trend observed across the rest of China and Asia, as reflected by the net warming of the global climate system (IPCC, 2014; Dong et al., 2017; Shi et al., 2018). However, within China, the studied CCR showed a different

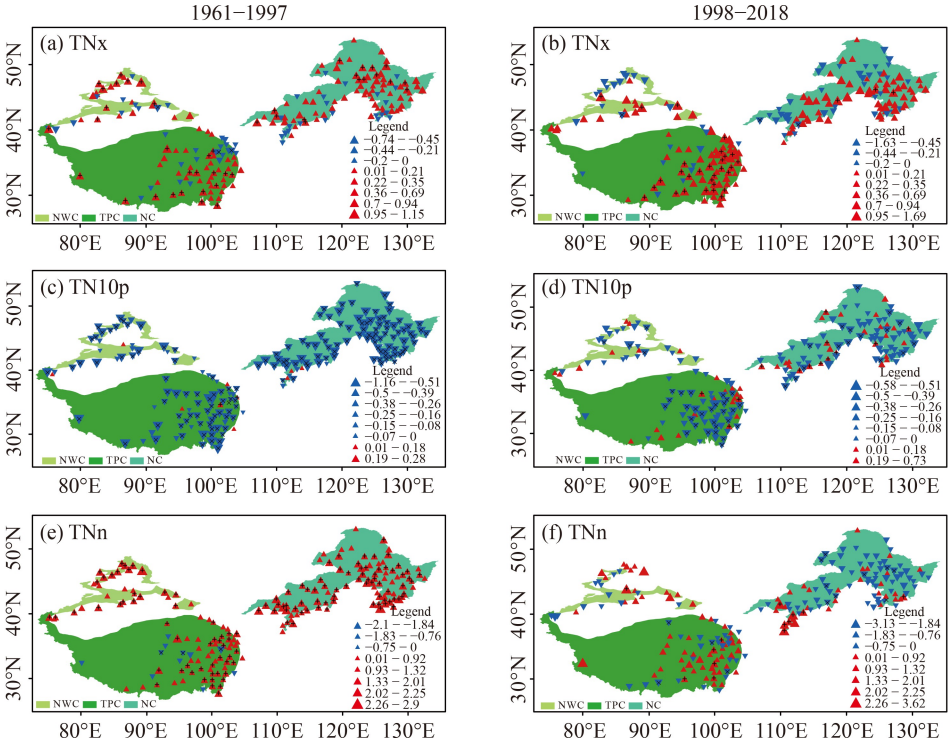

Fig. 8 The spatial distribution of annual extreme cold temperature trends between 1961–1997 and 1998–2018 for (a) (b) TNx, (c) (d) TN10p and (e) (f) TNn.

warming intensity from other regions in China. Table 4 indicates the difference in extreme temperature indices for the different regions of China from previous studies. It is apparent in Table 4 that the annual mean extreme temperature warming indices across CCR were greater than those observed around the Yangtze River (Niu et al., 2020) and across the whole China (Shi et al., 2018). When compared to other regions, we find that the cold extreme temperature indices have the greatest sensitivity. For example, TN10p and TNn of the Pearl River Basin were −1.23 days per decade and 0.44°C per decade from 1961 to 2015, but reached −2.74 days per decade and 0.63°C per decade across CCR during the same interval. Furthermore, the warming trend of extreme temperature indices on the Loess Plateau was obviously higher than that in CCR, except for the cold extremes. This specifically reflects the distinctive physical characteristics of high altitude and high latitude across CCR. Numerous studies confirm that the warming trends revealed by extreme temperature index across high-altitude/latitude regions are particularly sensitive, and that these regions act to amplify climate change, a finding that is consistent with our results (Dong et al., 2017; You et al., 2018; Li et al., 2020).

Within the CCR, the extreme temperature indices indicate a clear warming hiatus during 1998–2018. However, the annual mean extreme temperature indices of each of the sub-regions demonstrate different responses to the warming slowdown. In general, the extreme temperature indices across NWC and NC demonstrate a significant and consistent response to the warming hiatus. Specifically, during 1998–2018, the annual mean temperature (TXm and TNm), warm extremes (TX90p and TNx)

Table 4 The variations of temperature extremes across different regions in China

Region	China's cold regions	Yangtze River Basin (Niu et al., 2020)	Pearl River Basin (Liu et al., 2015)	Loess Plateau (Ding et al., 2020)	Southwestern China (Li et al., 2012)	China (Shi et al., 2018)
Period	1961–2018	1961–2014	1960–2012	1961–2018	1961–2008	1961–2015
TXm	0.23	0.16		0.29		0.21
TNm	0.43	0.20		0.39		0.37
TX90p	1.18	2.00	1.01	1.43	0.22	1.15
TNx	0.29	0.15	0.16	0.32	0.17	
TN10p	−2.74	−2.70	−1.23	−2.26	−0.37	−1.87
TNn	0.63	0.38	0.44	0.39	0.29	

and cold extremes (TN10p and TNn) all show a clear warming hiatus, even cooling across NWC and NC. However, the extreme temperature index across the TPC reveals an intensified warming trend except for the cold extreme temperature index (TN10p and TNn). Our observations indicate that TPC did not experience the warming hiatus, but instead the warming trend continued. Our results are consistent with the other studies of regional warming and extreme temperature trends across the Tibetan Plateau, Northwest China, and Northeast China (Duan and Xiao, 2015; Du et al., 2019; Li et al., 2020; Zhou et al., 2020).

Analysis on the seasonal scale reveals variable response in temperature extremes across the three cold regions to the warming hiatus of 1998–2018. Shen et al. (2018) showed that across China's mid-and high-latitudes, temperature variations in summer and winter are the critical factors for global warming slowdown. Hence, we likewise focus on summer and winter extremes in our discussion. In summer, the warm index across CCR reveals accelerating warming, with the exception of NC which experienced a warming hiatus. The cold index showed significant warming slowdown, resulting in cooling, except for TPC that underwent further warming. During winter, all extreme temperature indices for the three cold regions showed a robust warming slowdown and cooling trend. Our results suggest that the warming hiatus from 1998 to 2018 may be primarily due to the variations in winter extreme temperature index, which indicate a reduced frequency of "warm winter" events across CCR (Alexander et al., 2006; Caesar et al., 2011; Johnson et al., 2018; Ding et al., 2020). Across TPC, we find that the increased warming is mainly a result of variations in the warm extremes in summer. This is consistent with the characteristics of changes across Eurasia and North America (Gleisner et al., 2015; Li et al., 2015). A continuous increase in the intensity of temperature extremes in summer will lead to a continuous increase of heat waves. For example, from 1998 to 2018, TNx continued to warm at a rate of 0.49°C per decade (Fig. 6(c)), with important social and ecological impacts in the region (Sun et al., 2019).

Previous studies show that the geographic distribution and location of meteorological stations used in temperature index analysis may influence the resulting trends (You et al., 2008; Ding et al., 2019b, 2020). It is apparent (Table 5) that there is a significant positive correlation between trends of the extreme temperature index and altitude across the three cold regions. Overall, we find the higher the altitude, then the greater the amplitude of warming which is consistent with other studies (Niu et al., 2020; Ding et al., 2020). The correlation between extreme temperature index and latitude and altitude is, however, more complicated across the three cold regions. Extreme temperature index and longitude generally has a negative correlation in NC, except for the cold extremes; this might reflect that meteorological stations across NC are closer to the ocean, and are influenced by a moderating, maritime climate. Meteorological stations further inland are more influenced by a continental climate, resulting in larger extreme temperature variations.

Although human activities are responsible for increased aerosols and greenhouse gas emissions, there remain key regions that have critically witnessed a climate warming hiatus over the period from 1998 to 2018 (Chen and Dong, 2018). Many studies have explored the possible drivers for this warming slowdown, and current theories can be broadly divided into two broad sets of mechanisms: first, external forcing of the climate system, such as solar radiative forcing, volcanic activity, stratospheric water vapor and human activities. Kaufmann et al. (2011), for example, argued that periodic weakening of incoming solar radiation from 1998 to 2008 partially offset any increase in greenhouse gas concentrations, thereby driving a global warming hiatus. Likewise, Haywood et al. (2014) argue that aerosols from volcanic eruptions act to reduce incoming solar radiation reaching the ground, thereby leading to partial global cooling. However, cooling effects from volcanic eruptions have a relatively short duration and may be of insufficient magnitude to be impact on climate variability. Hansen et al. (2011) showed that aerosols produced by human activities have a direct impact on climate change, and Solomon et al. (2010) argued that a 10% drop in stratospheric water

Table 5 Correlation between trends of extreme temperature index and latitude, longitude and altitude across the three cold regions

Index	TPC			NWC			NC		
	Latitude	Longitude	Altitude	Latitude	Longitude	Altitude	Latitude	Longitude	Altitude
TXm	−0.002	−0.148	−0.007	0.196	**0.563****	0.030	−0.108	**−0.567****	**0.570****
TNm	−0.023	**−0.385****	**0.289****	0.228	−0.076	−0.286	0.098	−0.152	0.102
TX90p	−0.044	−0.026	**0.261***	−0.266	**0.485****	0.107	−0.084	**−0.526****	**0.505****
TNx	0.203	−0.081	**0.253****	0.301	0.281	0.060	0.111	**−0.398****	**0.338****
TN10p	**0.279****	**0.403****	**−0.280****	0.017	0.191	0.186	0.033	0.132	−0.081
TNn	−0.160	−0.159	0.231	0.187	−0.277	0.262	−0.103	0.135	−0.114

Notes: * is the 0.05 confidence level, and ** is the 0.01 confidence level.

vapor content after 2000 resulted in a global surface temperature drop of ~25% from 2000 to 2009. The second set of mechanisms concerns the internal variability of the climate system, and is mainly related to increased energy absorption by the deep ocean. Since 1971, about 94% of the heat received by the earth has been stored in the ocean, the majority of which has been absorbed in abyssal waters below 700 m depth; meanwhile, the upper ocean has not changed significantly, thereby leading to global surface warming slowdown (Balmaseda et al., 2013; IPCC, 2014; Meehl et al., 2013; Chen et al., 2014).

Recently, aerosol-radiation interactions and feedback caused by human activities have had significant influences on southeastern China. However, ocean surface atmospheric feedbacks and dynamic changes mainly affected northern China (Su and Dong, 2019). According to the Community Climate System Model version 4 simulation, the recent warming hiatus as well as ocean surface temperatures in the equatorial and eastern Pacific showed negative anomalies. Coincident positive anomalies in the mid-latitudes of the western and central Pacific suggested that the global warming hiatus may be related to the negative phase of the PDO (Kosaka and Xie, 2013; Meehl et al., 2013; Risbey et al., 2014). Although the PDO does impact upon the global warming slowdown, the underlying driver of this phenomenon is variations in the AMO. Chen et al. (2014) demonstrated that enhanced Atlantic meridional overturning circulation (AMOC) transports low-latitude seawater to the deep North Atlantic Ocean, leading to warming of the North Atlantic, which affects atmospheric circulation anomalies and cooling of the equatorial eastern Pacific. Hence, AMOC enhancement increases the heat capacity of the North Atlantic and reduces heat exchange with the atmosphere, impacting the PDO and thereby triggering global warming hiatus (England et al., 2014). The AMO reflects the intensity of AMOC changes (Chen and Tung, 2014). Our WTC results show the AMO in a positive phase relationship with TXm, TNm, TX90p and TNx across China's three cold regions before 1998. Moreover, the phase angle of the WTC gradually decreased from 270° to 0°, indicating that a positive correlation between the inter-annual and inter-decadal oscillating cycles gradually increased with

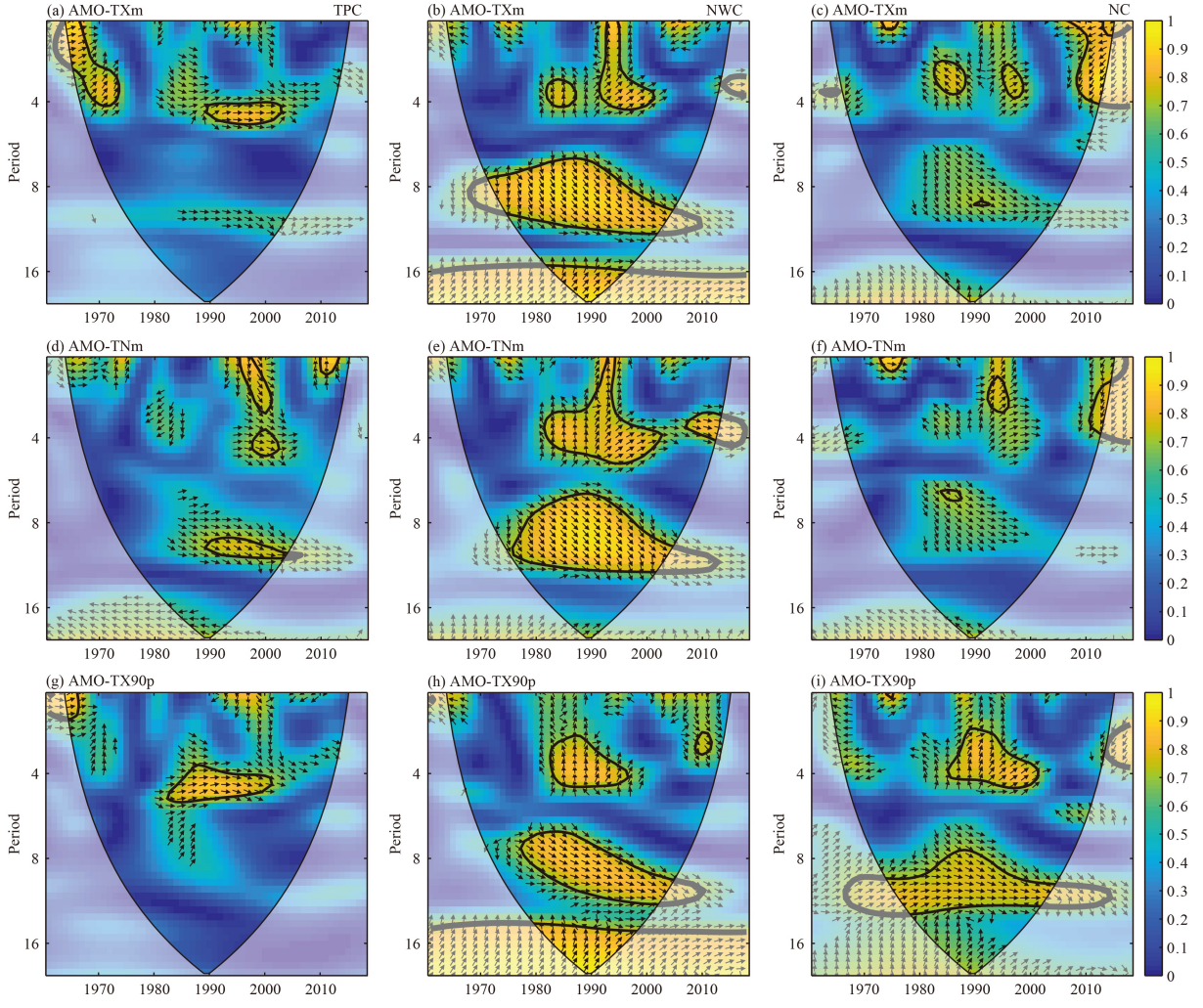

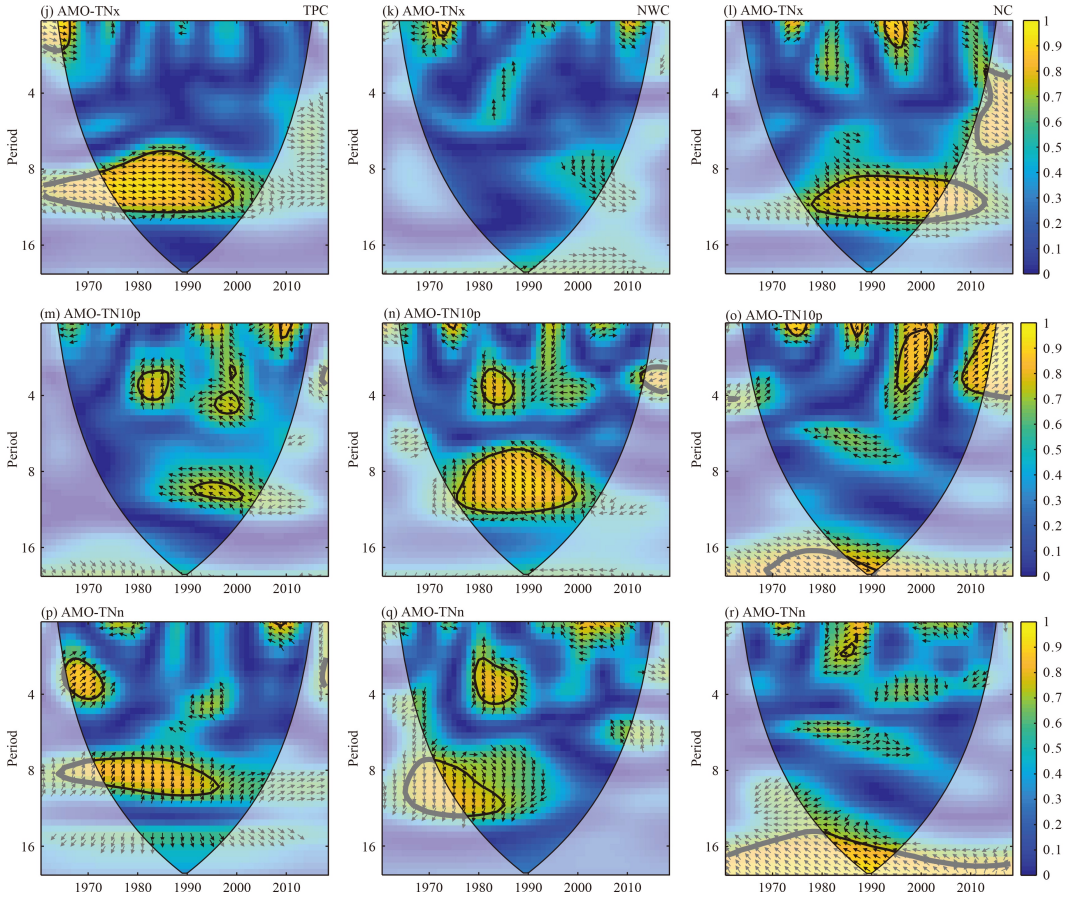

Fig. 9 Wavelet transform coherence for AMO and extreme temperature indices for China's three cold regions. The thick black contours denote the $p < 0.05$ confidence level, and the black line is the cone of influence - COI. Right-pointing arrows indicate in-phase signals, while left-pointing arrows indicate that the two signals are in anti-phase; down-pointing arrows indicate that the extreme temperature indices are ahead of the atmospheric index, while up-pointing arrows indicate that the extreme temperature indices lag behind the atmospheric index.

periodicities from 1 to 12 years (Fig. 9). After 1998, the phase angles of AMO and TXm, TNm, TX90p and TNx changed from 225° to 0°, with smaller, inter-annual oscillations dominating the record with a 1−5 year oscillation period, indicating the AMO has a significant impact on the four extreme temperature indices. In addition, compared with the other two cold regions, although the extreme temperature index across the TPC still has a significant positive correlation with AMO, wavelet energy is relatively small in the inter-annual oscillation period. The cold indices TN10p and TNn were correlated with the AMO in all three cold regions, and showed a strong negative relationship with a lagged response during 1980–2000 in the inter-annual and inter-decadal oscillation cycles (Fig. 9). In other words, the AMO was likely to have impacted the warming hiatus across CCR since 1998 through phase changes; this is consistent with other studies (McGregor et al., 2014; England et al., 2015; Ding et al., 2020).

Some studies also suggest that the AO has a strong influence on climate in the mid-high latitudes of the northern hemisphere. When AO is in anti-phase, cold flow into the mid- and high-latitudes is strengthened, and meridional exchange is enhanced, resulting in a decrease in temperature in the mid- and low-latitudes. On the contrary, when the AO is in phase, cold air is restricted from spreading southward (Sun et al., 2018; Zhou et al., 2020). WTC analyses reveal that TXm, TNm and TNx across the three cold regions have a significant positive correlation with AO ($P < 0.05$) on inter-annual and inter-decadal oscillation cycles with periodicities of 1–8 years, with the exception of the extreme temperature indices across the TPC which lag behind AO (Fig. 10). We found that prior to 1998, the AO had a significant positive correlation with TXm, TNm and TNx in NWC and NC ($P < 0.05$), and the phase angle gradually decreased from 90° to 0°, indicating that this positive relationship was gradually strengthening. However, after 1998, the phase angles of three extreme temperature indices gradually increased from 0° to 90°, indicating that the positive correlation was gradually weakening. For the cold index, AO showed strong negative correlations with TN10p of NWC and NC at inter-decadal scales, with a strong periodicity around 8 to 10 years, and the negative

correlation strengthened after 2000. Therefore, the phase change of AO around 1998 is likely to be another dominant factor leading to slowdown of warming across CCR. These findings are consistent with other studies (Huang et al., 2016; Zhang, 2016; Zhou et al., 2020).

Although anthropogenic activities have significantly influenced the climate in three cold regions, the warming hiatus since 1998 is more likely to be the result of natural variability of the climate system, in particular the AMO and AO. These large-scale ocean-atmosphere circulation patterns mainly affect the regional climate and environmental changes through their influence on the formation and movement of air masses, fronts, cyclones and anticyclones.

In the future, we should focus on using additional extreme temperature indices to explore the warming slowdown in China's cold regions. We should also analyze other factors that affect the warming hiatus in cold regions, such as the El Niño-Southern Oscillation index. Previous research has suggested that the strong El Niño event in 1998 may have affected the pattern of extreme temperature changes in China (Shen et al., 2018). In addition, as the "amplifier" of climate change, the Tibetan Plateau did not show warming slowdown during this period, but the physical mechanisms underlying this different response need further analysis.

5 Conclusions

The three cold regions in China have shown different responses to the global warming slowdown since 1998. NWC and NC showed an obvious warming slowdown and even a clear cooling trend in all extreme temperature indices, while the TPC only showed obvious changes in the cold index. The spatial distribution of regions with warming slowdown was not consistent across different extreme temperature indices. This indicated that different parts of the three cold regions have experienced different climate change patterns. Overall, the central and western regions of NWC and NC demonstrate a more significant slowdown in warming than other regions. However, across TPC, the most obvious accelerating warming and

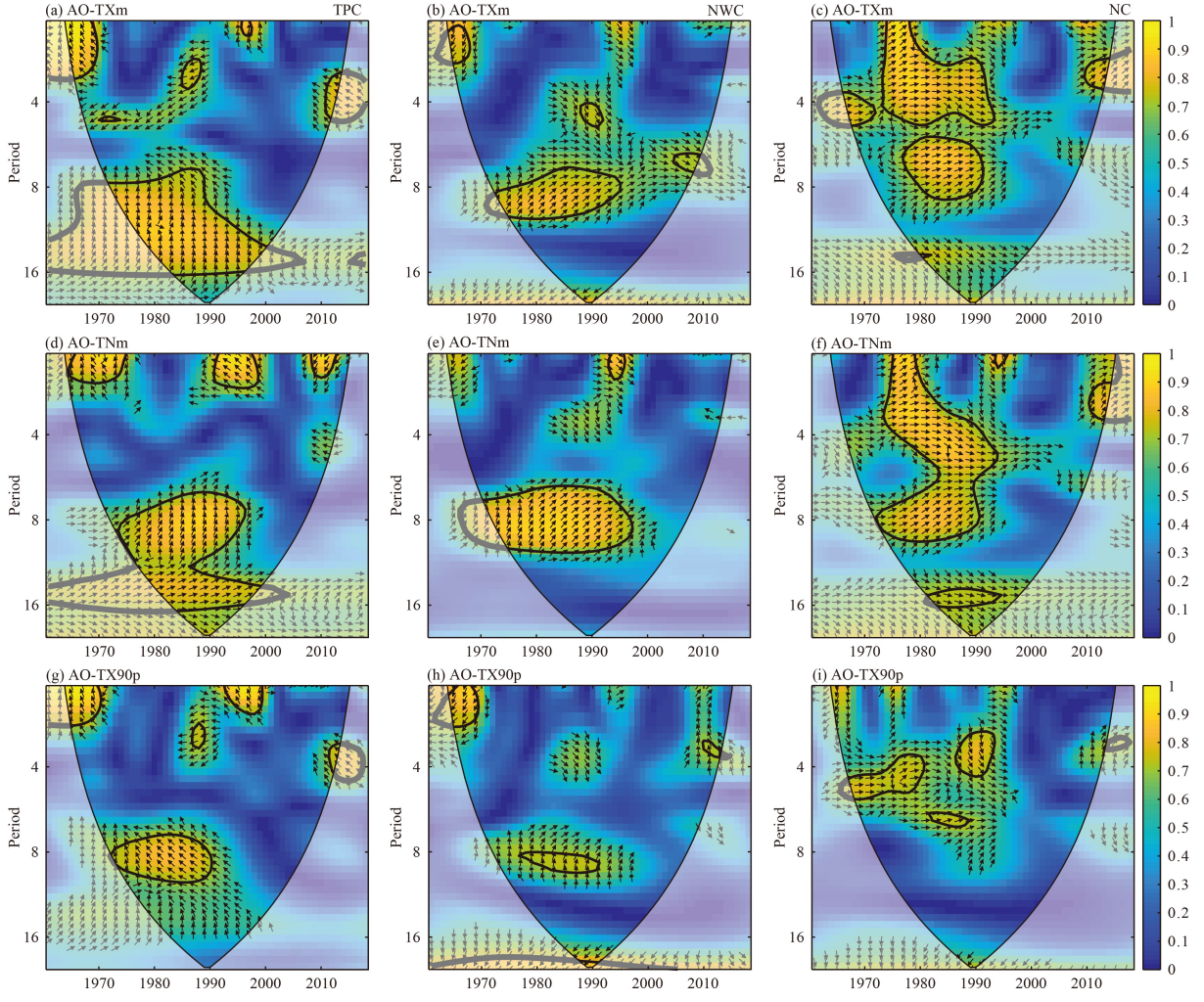

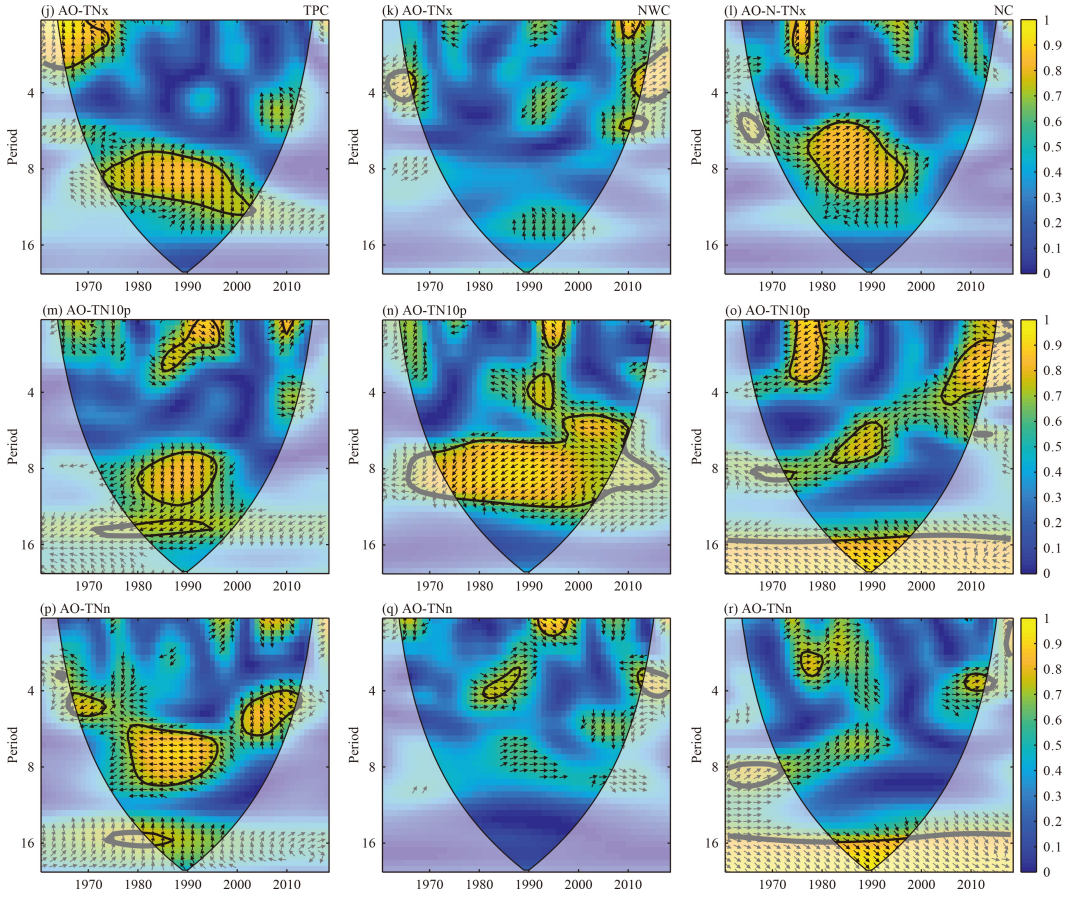

Fig. 10 Wavelet transform coherence for AO and extreme temperature indices across the three cold regions.

hiatus areas are located in the southeast.

During the recent warming slowdown period, all extreme temperature indices across all three cold regions showed an obvious warming hiatus during winter. In summer, the warm index across the entire CCR reveals significant accelerating warming except for NC, which experienced a slowdown in warming. Our cold index demonstrates an unequivocal warming hiatus, and even cooling, except for the TPC which continued to undergo accelerated warming.

The WTC results indicated that ocean-atmospheric circulation had a substantial impact on extreme temperature changes across CCR. Prior to 1998, the AMO and TXm, TNm, TX90p, and TNx for the three cold regions displayed varying inter-annual periodicities and a significant decadal in-phase periodicity. For the cold index, TN10p and TNn in all three regions showed a strong negative relationship with AMO and a lagged response from 1980 to 2000. Additionally, AO and TXm, TNm and TNx in all three cold regions showed a scattered inter-annual and inter-decadal oscillation periodicity ranging from 1 to 8 years. Furthermore, AO has a strong negative correlation with the TN10p cold index across NWC and NC at inter-decadal time scales, with a major period of about 8–10 years, and the negative correlation significantly strengthened after 2000. Overall, our results demonstrate that the warming hiatus across CCR from 1998 to 2018 was likely to have been primarily controlled by the AMO and AO.

References

Alexander L V, Zhang X, Peterson T C, Caesar J, Gleason B, Klein Tank A M G, Haylock M, Collins D, Trewin B, Rahimzadeh F, Tagipour A, Rupa Kumar K, Revadekar J, Griffiths G, Vincent L, Stephenson D B, Burn J, Aguilar E, Brunet M, Taylor M, New M, Zhai P, Rusticucci M, Vazquez-Aguirre J L (2006). Global observed changes in daily climate extremes of temperature and precipitation. J Geophys Res, 111(D5): D05109

An W, Hou S, Zhang W, Wu S, Xu H, Pang H, Wang Y, Liu Y (2016). Possible recent warming hiatus on the northwestern Tibetan Plateau derived from ice core records. Sci Rep, 6(1): 32813

Balmaseda M A, Trenberth K E, Källén E (2013). Distinctive climate signals in reanalysis of global ocean heat content. Geophys Res Lett, 40(9): 1754–1759

Bubeck P, Dillenardt L, Alfieri L, Feyen L, Thieken A H, Kellermann

P (2019). Global warming to increase flood risk on European railways. Clim Change, 155(1): 19–36

Caesar J, Alexander L V, Trewin B, Tse-ring K, Sorany L, Vuniyayawa V, Keosavang N, Shimana A, Htay M M, Karmacharya J, Jayasinghearachchi D A, Sakkamart J, Soares E, Hung L T, Thuong L T, Hue C T, Dung N T T, Hung P V, Cuong H D, Cuong N M, Sirabaha S (2011). Changes in temperature and precipitation extremes over the Indo-Pacific region from 1971 to 2005. Int J Climatol, 31(6): 791–801

Cai D, You Q, Fraedrich K, Guan Y (2017). Spatiotemporal temperature variability over the Tibetan Plateau: altitudinal dependence associated with the global warming hiatus. J Clim, 30(3): 969–984

Chen H, Sun J (2015). Changes in climate extreme events in China associated with warming. Int J Climatol, 35(10): 2735–2751

Chen R, Kang E, Ji X, Yang J, Yang Y (2006). Cold regions in China. Cold Reg Sci Technol, 45(2): 95–102

Chen W, Dong B (2018). Anthropogenic impacts on recent decadal change in temperature extremes over China: relative roles of greenhouse gases and anthropogenic aerosols. Clim Dyn, 52(5−6): 3643–3660

Chen X, Tung K K (2014). Varying planetary heat sink led to global-warming slowdown and acceleration. Science, 345(6199): 897–903

Chen Y, Deng H, Li B, Li Z, Xu C (2014). Abrupt change of temperature and precipitation extremes in the arid region of northwest China. Quat Int, 336: 35–43

Curtis S, Fair A, Wistow J, Val D V, Oven K (2017). Impact of extreme weather events and climate change for health and social care systems. Environ Health, 16(S1 Suppl 1): 128

Deng H, Chen Y, Shi X, Li W, Wang H, Zhang S, Fang G (2014). Dynamics of temperature and precipitation extremes and their spatial variation in the arid region of northwest China. Atmos Res, 138: 346–355

Diffenbaugh N S, Singh D, Mankin J S, Horton D E, Swain D L, Touma D, Charland A, Liu Y, Haugen M, Tsiang M, Rajaratnam B (2017). Quantifying the influence of global warming on unprecedented extreme climate events. Proc Natl Acad Sci USA, 114(19): 4881–4886

Ding Y, Zhang S, Zhao L, Li Z, Kang S (2019a). Global warming weakening the inherent stability of glaciers and permafrost. Sci Bull (Beijing), 64(4): 245–253

Ding Z, Lu R, Wang Y (2019b). Spatiotemporal variations in extreme precipitation and their potential driving factors in non-monsoon regions of China during 1961–2017. Environ Res Lett, 14(2): 024005

Ding Z, Pu J, Meng L, Lu R, Wang Y, Li Y, Dong Y, Wang S (2020). Asymmetric trends of extreme temperature over the Loess Plateau during 1998–2018. Int J Climatol, 41(S1): E1663–E1685

Ding Z, Wang Y, Lu R (2018). An analysis of changes in temperature extremes in the Three River Headwaters region of the Tibetan Plateau during 1961–2016. Atmos Res, 209(SEP): 103–114

Donat M G, Lowry A L, Alexander L V, O'Gorman P A, Maher N (2016). More extreme precipitation in the world's dry and wet regions. Nat Clim Chang, 6(5): 508–513

Dong S, Sun Y, Aguilar E, Zhang X, Peterson T C, Song L, Zhang Y (2017). Observed changes in temperature extremes over Asia and their attribution. Clim Dyn, 51(1−2): 339–353

Du Q, Zhang M, Wang S, Che C, Ma R, Ma Z (2019). Changes in air temperature over China in response to the recent global warming hiatus. J Geogr Sci, 29(4): 496–516

Duan A, Xiao Z (2015). Does the climate warming hiatus exist over the Tibetan Plateau? Sci Rep, 5(1): 13711

Easterling D R, Wehner M F (2009). Is the climate warming or cooling? Geophys Res Lett, 36(8): L08706

England M H, Kajtar J B, Maher N (2015). Robust warming projections despite the recent hiatus. Nat Clim Chang, 5(5): 394–396

England M H, McGregor S, Spence P, Meehl G A, Timmermann A, Cai W, Gupta A S, McPhaden M J, Purich A, Santoso A (2014). Recent intensification of wind-driven circulation in the Pacific and the ongoing warming hiatus. Nat Clim Chang, 4(3): 222–227

Fenner D, Holtmann A, Krug A, Scherer D (2019). Heat waves in Berlin and Potsdam, Germany – long-term trends and comparison of heat wave definitions from 1893 to 2017. Int J Climatol, 39(4): 2422–2437

Fu Q, Zhou Z, Li T, Liu D, Hou R, Cui S, Yan P (2018). Spatiotemporal characteristics of droughts and floods in northeastern China and their impacts on agriculture. Stochastic Environ Res Risk Assess, 32(10): 2913–2931

Fyfe J C, Gillett N P, Zwiers F W (2013). Overestimated global warming over the past 20 years. Nat Clim Chang, 3(9): 767–769

Fyfe J C, Meehl G A, England M H, Mann M E, Santer B D, Flato G M, Hawkins E, Gillett N P, Xie S P, Kosaka Y, Swart N C (2016). Making sense of the early-2000s warming slowdown. Nat Clim Chang, 6(3): 224–228

Garfinkel C I, Son S W, Song K, Aquila V, Oman L D (2017). Stratospheric variability contributed to and sustained the recent hiatus in Eurasian winter warming. Geophys Res Lett, 44(1): 374–382

Gleisner H, Thejll P, Christiansen B, Nielsen J (2015). Recent global warming hiatus dominated by low-latitude temperature trends in surface and troposphere data. Geophys Res Lett, 42(2): 510–517

Grinsted A, Moore J C, Jevrejeva S (2004). Application of the cross wavelet transform and wavelet coherence to geophysical time series. Nonlinear Process Geophys, 11(5/6): 561–566

Guo H, Bao A, Liu T, Jiapaer G, Ndayisaba F, Jiang L, Kurban A, De Maeyer P (2018). Spatial and temporal characteristics of droughts in Central Asia during 1966−2015. Sci Total Environ, 624: 1523–1538

Hansen J, Sato M, Kharecha K, von Schuckmann K (2011). Earth's energy imbalance and implications. Atmos Chem Phys, 11(24): 13421–13449

Haywood J M, Jones A, Jones G S (2014). The impact of volcanic eruptions in the period 2000–2013 on global mean temperature trends evaluated in the HadGEM2-ES climate model. Atmos Sci Lett, 15(2): 92–96

Huang J, Xie Y, Guan X, Li D, Ji F (2016). The dynamics of the warming hiatus over the Northern Hemisphere. Clim Dyn, 48(1−2): 429–446

Huang J, Zhang X, Zhang Q, Lin Y, Hao M, Luo Y, Zhao Z, Yao Y, Chen X, Wang L, Nie S, Yin Y, Xu Y, Zhang J (2017a). Recently amplified arctic warming has contributed to a continual global

warming trend. Nat Clim Chang, 7(12): 875–879

Huang Q, Zhang Q, Singh V P, Shi P, Zheng Y (2017b). Variations of dryness/wetness across China: changing properties, drought risks, and causes. Global Planet Change, 155: 1–12

IPCC (2014). Summary for Policymakers. In: Climate Change 2013 – The Physical Science Basis: Working Group I Contribution to the Fifth Assessment Report of the Intergovernmental Panel on Climate Change. Cambridge: Cambridge University Press

Jevrejeva S, Moore J C, Grinsted A (2003). Influence of the Arctic Oscillation and El Niño-Southern Oscillation (ENSO) on ice conditions in the Baltic Sea: the wavelet approach. J Geophys Res D Atmospheres, 108(D21): 4677

Johnson N C, Xie S P, Kosaka Y, Li X (2018). Increasing occurrence of cold and warm extremes during the recent global warming slowdown. Nat Commun, 9(1): 1724

Karl T R, Arguez A, Huang B, Lawrimore J H, McMahon J R, Menne M J, Peterson T C, Vose R S, Zhang H M (2015). Possible artifacts of data biases in the recent global surface warming hiatus. Science, 348(6242): 1469–1472

Kaufmann R K, Kauppi H, Mann M L, Stock J H (2011). Reconciling anthropogenic climate change with observed temperature 1998–2008. Proc Natl Acad Sci, 108(29): 11790–11793

Kerr R A (2009). What happened to global warming? Scientists say just wait a bit. Science, 326(5949): 28–29

Kosaka Y, Xie S P (2013). Recent global-warming hiatus tied to equatorial Pacific surface cooling. Nature, 501(7467): 403–407

Li C, Stevens B, Marotzke J (2015). Eurasian winter cooling in the warming hiatus of 1998–2012. Geophys Res Lett, 42(19): 8131–8139

Li L, Zha Y (2018). Mapping relative humidity, average and extreme temperature in hot summer over China. Sci Total Environ, 615: 875–881

Li X, Cheng G (1999). A GIS-aided response model of high-altitude permafrost to global change. Sci China Ser D Earth Sci, 42(1): 72–79

Li X, You Q, Ren G, Wang S, Zhang Y, Yang J, Zheng G (2019). Concurrent droughts and hot extremes in northwest China from 1961 to 2017. Int J Climatol, 39(4): 2186–2196

Li Z, Ding Y, Chen A, Zhang Z, Zhang S (2020). The hiatus phenomenon and characteristics in the climate change in northwest China from 1960 to 2019. Acta Geogr Sin, 75(9): 1845–1859

Li Z, He Y, Wang P, Theakstone W H, An W, Wang X, Lu A, Zhang W, Cao W (2012). Changes of daily climate extremes in south-western China during 1961–2008. Global Planet Change, 80–81: 255–272

Liu Q, Wu X, Chen X, Yang B (2015). Temporal and spatial variation characteristics of extreme temperature in the Pearl River Basin from 1960 to 2012. Journal of Natural Resources, 30(8): 1356–1366

McGregor S, Timmermann A, Stuecker M F, England M H, Merrifield M, Jin F F, Chikamoto Y (2014). Recent Walker circulation strengthening and Pacific cooling amplified by Atlantic warming. Nat Clim Chang, 4(10): 888–892

Medhaug I, Stolpe M B, Fischer E M, Knutti R (2017). Reconciling controversies about the 'global warming hiatus'. Nature, 545(7652): 41–47

Meehl G A, Hu A, Arblaster J M, Fasullo J, Trenberth K E (2013). Externally forced and internally generated decadal climate variability associated with the interdecadal Pacific Oscillation. J Clim, 26(18): 7298–7310

Niu Z, Wang L, Fang L, Li J, Yao R (2020). Analysis of spatiotemporal variability in temperature extremes in the Yellow and Yangtze River basins during 1961–2014 based on high-density gauge observations. Int J Climatol, 40(1): 1–21

Pakalidou N, Karacosta P (2018). Study of very long-period extreme precipitation records in Thessaloniki, Greece. Atmos Res, 208: 106–115

Qin D, Ding Y, Xiao C, Kang S, Ren J, Yang J, Zhang S (2018). Cryospheric science: research framework and disciplinary system. Natl Sci Rev, 5(2): 255–268

Rajaratnam B, Romano J, Tsiang M, Diffenbaugh N S (2015). Debunking the climate hiatus. Clim Change, 133(2): 129–140

Ren G, Ding Y, Zhao Z, Zheng J, Wu T, Tang G, Xu Y (2012). Recent progress in studies of climate change in China. Adv Atmos Sci, 29(5): 958–977

Risbey J S, Lewandowsky S, Langlais C, Monselesan D P, O'Kane T J, Oreskes N (2014). Well-estimated global surface warming in climate projections selected for ENSO phase. Nat Clim Chang, 4(9): 835–840

Sen P K (1968). Estimates of the regression coefficient based on Kendall's Tau. J Am Stat Assoc, 63(324): 1379–1389

Shen X, Jiang M, Lu X, Liu X, Liu B, Zhang J, Wang X, Tong S, Lei G, Wang S, Tong C, Fan H, Tian K, Wang X, Hu Y, Xie Y, Ma M, Zhang S, Cao C, Wang Z (2021). Aboveground biomass and its spatial distribution pattern of herbaceous marsh vegetation in China. Sci China Earth Sci, 64(7): 1115–1125

Shen X, Liu B, Jiang M, Lu X (2020). Marshland loss warms local land surface temperature in China. Geophys Res Lett, 47(6): e2020GL087648

Shen X, Liu B, Lu X (2018). Weak cooling of cold extremes versus continued warming of hot extremes in China during the recent global surface warming hiatus. J Geophys Res D Atmospheres, 123(8): 4073–4087

Shi J, Cui L, Ma Y, Du H, Wen K (2018). Trends in temperature extremes and their association with circulation patterns in China during 1961–2015. Atmos Res, 212: 259–272

Slingo J (2013). The Recent Pause in Global Warming Parts 1–3 Rep. Exeter: The Met Office

Solomon S, Rosenlof K H, Portmann R W, Daniel J S, Davis S M, Sanford T J, Plattner G K (2010). Contributions of stratospheric water vapor to decadal changes in the rate of global warming. Science, 327(5970): 1219–1223

Song L, Wu R (2019). Different cooperation of the Arctic Oscillation and the Madden-Julian Oscillation in the East Asian cold events during early and late winter. J Geophys Res D Atmospheres, 124 (9): 4913–4931

Su Q, Dong B (2019). Recent decadal changes in heat waves over China: drivers and mechanisms. J Clim, 32(14): 4215–4234

Sun X, Ren G, Ren Y, Fang Y, Liu Y, Xue X, Zhang P (2018). A remarkable climate warming hiatus over northeast China since 1998. Theor Appl Climatol, 133(1−2): 579–594

Supari, Tangang F, Juneng L, Aldrian E (2017). Observed changes in extreme temperature and precipitation over Indonesia. Int J Climatol, 37(4): 1979–1997

Swain D L, Horton D E, Singh D, Diffenbaugh N S (2016). Trends in atmospheric patterns conducive to seasonal precipitation and temperature extremes in California. Sci Adv, 2(4): e1501344

Tong S, Li X, Zhang J, Bao Y, Bao Y, Na L, Si A (2019). Spatial and temporal variability in extreme temperature and precipitation events in Inner Mongolia (China) during 1960-2017. Sci Total Environ, 649: 75–89

Torrence C, Compo G P (1998). A practical guide to wavelet analysis. Bull Am Meteorol Soc, 79(1): 61–78

Trenberth K E (2015). Has there been a hiatus? Science, 349(6249): 691–692

Wang S, Zhang M, Wang B, Sun M, Li X (2013). Recent changes in daily extremes of temperature and precipitation over the western Tibetan Plateau, 1973–2011. Quat Int, (313−314): 110−117

Wang Y, Ding Z, Ma Y (2019). Spatial and temporal analysis of changes in temperature extremes in the non-monsoon region of China from 1961 to 2016. Theor Appl Climatol, 137(3−4): 2697–2713

Wang Y, Shen X, Jiang M, Tong S, Lu X (2021). Spatiotemporal change of aboveground biomass and its response to climate change in marshes of the Tibetan Plateau. Int J Appl Earth Obs Geoinf, 102: 102385

Wen X, Wu X, Gao M (2017). Spatiotemporal variability of temperature and precipitation in Gansu Province (northwest China) during 1951–2015. Atmos Res, 197: 132–149

Winslow L A, Leach T H, Rose K C (2018). Global lake response to the recent warming hiatus. Environ Res Lett, 13(5): 054005

Yang Z, Liu X, Zeng Q, Chen Z (2000). Hydrology in Cold Regions of China. Beijing: Science Press

You Q, Jiang Z, Wang D, Pepin N, Kang S (2018). Simulation of temperature extremes in the Tibetan Plateau from CMIP5 models and comparison with gridded observations. Clim Dyn, 51(1−2): 355–369

You Q, Kang S, Pepin N, Yan Y (2008). Relationship between trends in temperature extremes and elevation in the eastern and central Tibetan Plateau, 1961–2005. Geophys Res Lett, 35(4): L04704

You Q, Ren G, Fraedrich K, Kang S, Ren Y, Wang P (2013). Winter temperature extremes in China and their possible causes. Int J Climatol, 33(6): 1444–1455

Zhang L (2016). The roles of external forcing and natural variability in global warming hiatuses. Clim Dyn, 47(9−10): 3157–3169

Zhang X, Alexander L, Hegerl G C, Jones P, Tank A K, Peterson T C, Trewin B, Zwiers F W (2011). Index for monitoring changes in extremes based on daily temperature and precipitation data. WIREs Clim Change, 2(6): 851–870

Zhou Z, Shi H, Fu Q, Li T, Gan T Y, Liu S, Liu K (2020). Is the cold region in northeast China still getting warmer under climate change impact? Atmos Res, 237: 104864

Zhu J, Huang G, Baetz B, Wang X, Cheng G (2018). Climate warming will not decrease perceived low-temperature extremes in China. Clim Dyn, 52(9−10): 5641–5656